Cell Imaging

DOI: 10.1002/anie.201101659

Noninvasive Photoacoustic Microscopy of Living Cells in Two and Three Dimensions through Enhancement by a Metabolite Dye**

Yu Zhang, Xin Cai, Yu Wang, Chi Zhang, Li Li, Sung-Wook Choi, Lihong V. Wang, and Younan Xia**

Photoacoustic microscopy (PAM) is based on the detection of acoustic waves from an object that absorbs pulsed or intensity-modulated optical irradiation,[1] and it has become an attractive modality for examining tissues in a noninvasive manner with high resolution and penetration depth. The nonionizing waves used for photoacoustic imaging impose no adverse effects on tissues, in contrast with ionizing X-rays in micro-computer tomography.[1] The natural pigments such as melanin in melanoma cells and hemoglobin in erythrocytes can serve as endogenous optical absorption contrast agents and have enabled label-free PAM imaging of melanoma and blood vessels with relatively high sensitivity.[2–4] Recently, we demonstrated PAM imaging and quantification of melanoma cells in 3D inverse opal scaffolds up to 1.5 mm thick for application in tissue engineering.[5] However, most other types of cells have no intrinsic pigments and thus cannot be readily detected by PAM. Cells engineered with fluorescent proteins may give photoacoustic signals,[6] but the signal intensities are usually low because of their small extinction coefficients ($< 50000\,\mathrm{M^{-1}cm^{-1}}$). Li et al. recently demonstrated in vivo PAM imaging of cells that were transfected with lacZ gene and then stained with 5-bromo-4-chloro-3-indolyl-beta-D-galactopyranoside (X-gal).[7] Gold-based nanoparticles have also been shown to give extremely strong photoacoustic signals,[8,9] but their biodistribution and potential toxicity are of concern.

Here, we introduce a contrast agent based on 1-(4,5-dimethyl-2-thiazolyl)-3,5-diphenylformazan (MTT formazan) for stable and nontoxic staining of various types of cells, allowing high-resolution PAM imaging. More importantly, we demonstrated noninvasive and nondestructive imaging of cells with the staining method to spatially resolve individual cells or cell clusters, as well as their distribution, proliferation, and invasion profiles inside 3D porous scaffolds. To our knowledge, there is no report on contrast agents for photoacoustic imaging that can be applied to essentially all types of cells.

The key component of our approach is MTT, a tetrazole, that can be metabolized and reduced to MTT formazan in living cells (Figure 1a).[10–13] The MTT assay has long been used to biochemically evaluate cell viability, metabolic activity, and proliferation profile. The concentration of MTT formazan is determined by extracting it from cells with an organic solvent and then measuring the optical density using a spectrophotometer. In general, the optical

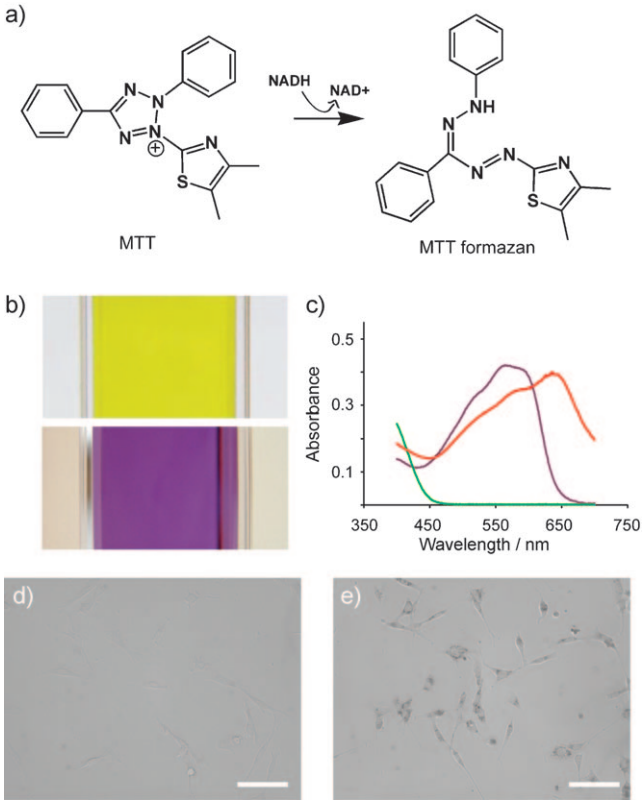

Figure 1. a) Reduction metabolism of the 1-(4,5-dimethyl-2-thiazolyl)-3,5-diphenyltetrazolium cation (MTT) inside a living cell; b) photographs of an MTT solution in phosphate-buffered saline (PBS; top) and an MTT formazan solution in 1-propanol (bottom); c) UV/Vis absorption spectra of the MTT solution in PBS (green curve), the MTT formazan solution in 1-propanol (purple curve), and the MTT formazan crystals suspended in PBS (red curve); bright-field optical micrographs showing fibroblasts incubated in the d) absence and e) presence of 0.05 w/v% MTT for 3 h (scale bars: 100 μm).

[*] Y. Zhang, X. Cai, Y. Wang, C. Zhang, L. Li, Dr. S.-W. Choi, Prof. L. V. Wang, Prof. Y. Xia
Department of Biomedical Engineering, Washington University
Saint Louis, MO 63130 (USA)
E-mail: lhwang@seas.wustl.edu
xia@biomed.wustl.edu

[**] This work was supported in part by the NIH Director's Pioneer Award (DP1 OD000798) and startup funds from Washington University in St. Louis (to Y.X.). This work was also sponsored by grants of the NIH (numbers R01 EB000712, R01 EB008085, and U54 CA136398 to L.V.W.). Part of the research was performed at the Nano Research Facility, a member of the National Nanotechnology Infrastructure Network (NNIN), which is supported by the NSF under award ECS-0335765.

Supporting information for this article is available on the WWW under http://dx.doi.org/10.1002/anie.201101659.

density is linearly proportional to the number of metabolically active cells. The MTT formazan is insoluble in water but soluble in a number of organic solvents. The MTT formazan solution in 1-propanol has a purple color (Figure 1b, bottom), with a broad, strong absorption in the spectral region of 500–620 nm, and a peak at around 560 nm (Figure 1c, purple line). There is also a linear relationship between the absorbance and the concentration of MTT formazan in 1-propanol (see Figure S1 in the Supporting Information). In contrast, the MTT solution in phosphate-buffered saline (PBS) shows a yellowish color (Figure 1b, top) with absorption below 450 nm (Figure 1c, green line).

Since MTT formazan crystals also show a purple color, it is not unreasonable to assume that their absorption spectra are similar to what is observed for their solution in 1-propanol. Indeed, the crystals suspension in PBS shows strong absorption in the spectral region of 500–700 nm, with a peak at around 650 nm (Figure 1c, red line). This red shift in the absorption band relative to the band of individual molecules in 1-propanol is probably because of the coupling of molecular transition dipoles.[14] As a result, the MTT formazan crystals generated inside living cells can be directly used to greatly enhance the contrast for conventional optical microscopy. Except for a few types of cells (e.g., melanoma cells and erythrocytes), most other cells (e.g., fibroblasts) show very little contrast under an optical microscope and can barely be observed (Figure 1d). However, after 3 h of incubation with MTT in a conventional culture medium, the cells could be easily resolved with sharp contrast because the metabolite MTT formazan strongly absorbs visible light and provides good contrast for bright-field imaging (Figure 1e). In this case, the MTT formazan is more or less equivalent to the natural pigment in melanoma cells or erythrocytes, suggesting its potential use as a contrast agent for PAM. To our knowledge, there is no report on the use of MTT formazan as a contrast agent for PAM of living cells.

We then demonstrated the suitability of MTT formazan as a contrast agent for PAM of cells cultured on 2D substrates. In a typical experiment, fibroblasts were incubated with MTT in a culture medium for 3 h under normal conditions (37 °C and 5% CO_2). Afterwards, the cells were briefly fixed and fluorescently stained for f-actin and imaged with a confocal-PAM hybrid system that can measure both fluorescence contrasts and optical absorption.[15] The confocal and PAM images (Figure 2a,c,e) indicate that nearly all the cells stained with MTT formazan were detected by PAM. The undetected cells are presumably due to the fact that they were dead prior to MTT treatment, thus preventing conversion of MTT to MTT formazan (Figure 2b,d,f).

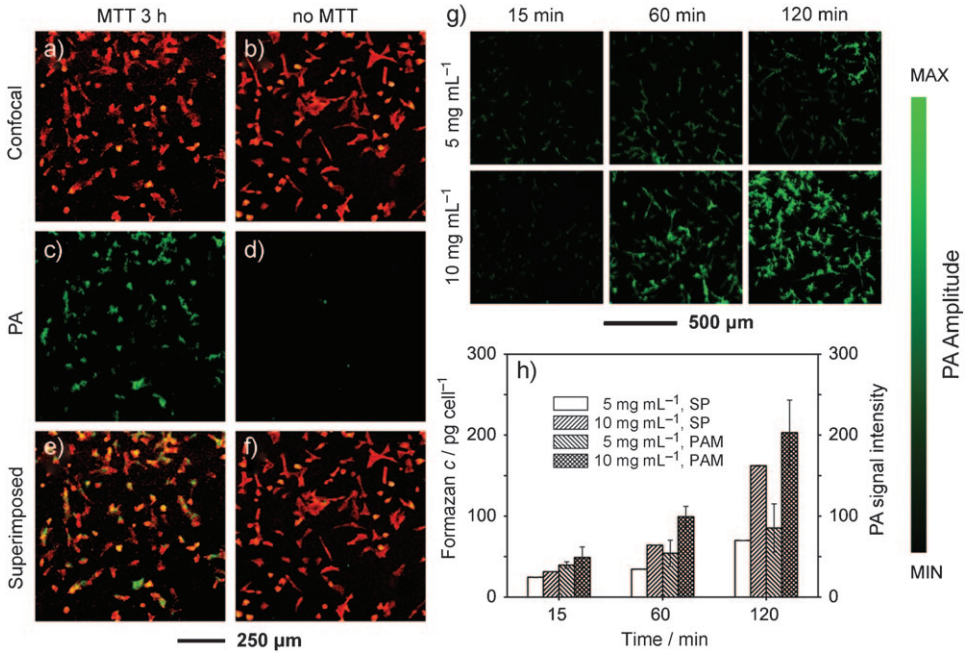

Figure 2. a,b) Confocal microscopy images and c,d) photoacoustic microscopy (PAM) images of fibroblasts cultured on cover glasses. The cells were incubated in the a,c) presence and b,d) absence of MTT, respectively, for 3 h, followed by fixation and staining for f-actin with Alexa 568-phalloidin. e,f) Superimposed images, indicating that essentially all the cells were stained by MTT formazan. g) PAM images of fibroblasts cultured on cover glasses in the presence of MTT at the indicated concentration and duration of time. The photoacoustic (PA) signal amplitude increased as the concentration of MTT and the incubation time were increased. h) The amount of MTT formazan (picogram, pg) and PA signal intensity per cell as a function of MTT concentration and incubation time. After PAM imaging, the MTT formazan in each sample was extracted by dissolution with 1-propanol and then quantified using a spectrophotometer. The MTT formazan concentrations were calculated from the calibration curve (see Figure S1 in the Supporting Information) and then divided by the cell numbers ($n=3$). The PA signal intensity per cell was calculated from the PA image and cell number ($n=4$). Data are presented as mean value ± standard deviation (SP = spectrophotometry).

The intensity of the collected photoacoustic signals is dependent on both the concentration of MTT and the incubation time because these two parameters determine the amount of MTT formazan generated inside each cell. To quantify these correlations, we added 40 µL of 5 mg mL^{-1} or 10 mg mL^{-1} MTT solution to the culture medium in each well containing 5×10^4 fibroblasts and incubated for 15, 60, and 120 min. The PAM images (Figure 2g) indicate that, at 15 min of incubation, both concentrations gave low signals of similar intensity, presumably because of the limited uptake and/or metabolic conversion of MTT by the cells within the short period of time. As the incubation time was prolonged, the signal intensity increased; similarly, the signal intensity was

stronger at a higher concentration of MTT under the same incubation time.

Immediately after each PAM scan, we extracted the formazan crystals from the cells by dissolution with 1-propanol and then quantified the amount using a spectrophotometer. The amount of MTT formazan per cell was calculated based on the calibration curve (see Figure S1 in the Supporting Information) and the number of cells in each well. As shown in Figure 2 h, the calculated MTT formazan amount per cell correlated well with the PAM image. The amount of formazan per cell for 10 mg mL^{-1} MTT was approximately twice of that for 5 mg mL^{-1} with incubation times up to 120 min except for the initial time point (15 min), where the two samples only showed a minor difference. At fixed concentrations of 5 and 10 mg mL^{-1}, the amount of formazan per cell increased with incubation time. We also calculated the photoacoustic (PA) signal intensity per cell from the PA image. Interestingly, the PA signal intensity per cell showed a trend similar to what was observed in the spectroscopic measurements (Figure 2 h).

We also followed the cellular metabolism of MTT as a function of incubation time by imaging the samples with optical microscopy (see Figure S2 a–f in the Supporting Information). In a 24-well plate, cells were seeded with the same density (5×10^4 fibroblasts per well). After culture for 12 h, 40 μL of 5 mg mL^{-1} MTT was added to each well. The cells showed increasing accumulation of MTT formazan with prolonged incubation time, and no significant exocytosis of MTT formazan crystals was observed up till $t=3$ h. Starting from $t=4$ h, however, exocytosis became obvious. At $t=12$ h post MTT addition, a large amount of the MTT formazan crystals were released by exocytosis in the form of small needles (see Figure S2 g in the Supporting Information). Moreover, once the needle-like MTT formazan crystals had been fully released by exocytosis and detached from the cells, they would float on top of the culture medium. Live/dead staining revealed that the cells were still alive in the process of exocytosis (green color, see Figure S2 h in the Supporting Information). Furthermore, we performed live/dead staining at each time point post MTT addition, and we found that >99% of the cells were alive in all cases, similar to the control group without MTT treatment.

We further explored the use of this staining method for 3D cellular imaging, which is highly sought-after in tissue engineering. We seeded fibroblasts in poly(D,L-lactide-*co*-glycolide) (PLGA) inverse opal scaffolds that exhibited a uniform pore size and structure and high interconnectivity to facilitate nutrient/waste transport and cell migration (see Figure S4 in the Supporting Information).[16,17] At day 5, the cell/scaffold constructs were incubated with MTT for 3 h, briefly rinsed with PBS, and immediately scanned with PAM. Maximum amplitude projection (MAP) images from the top and the side revealed the spatial distribution of cells in the 3D space of the scaffold with a penetration depth of over 1.2 mm (Figure 3 a, black dots). More importantly, we were able to render 3D cell distribution from the volumetric PAM data (Figure 3 b). To evaluate the ability of MTT to stain cells in a

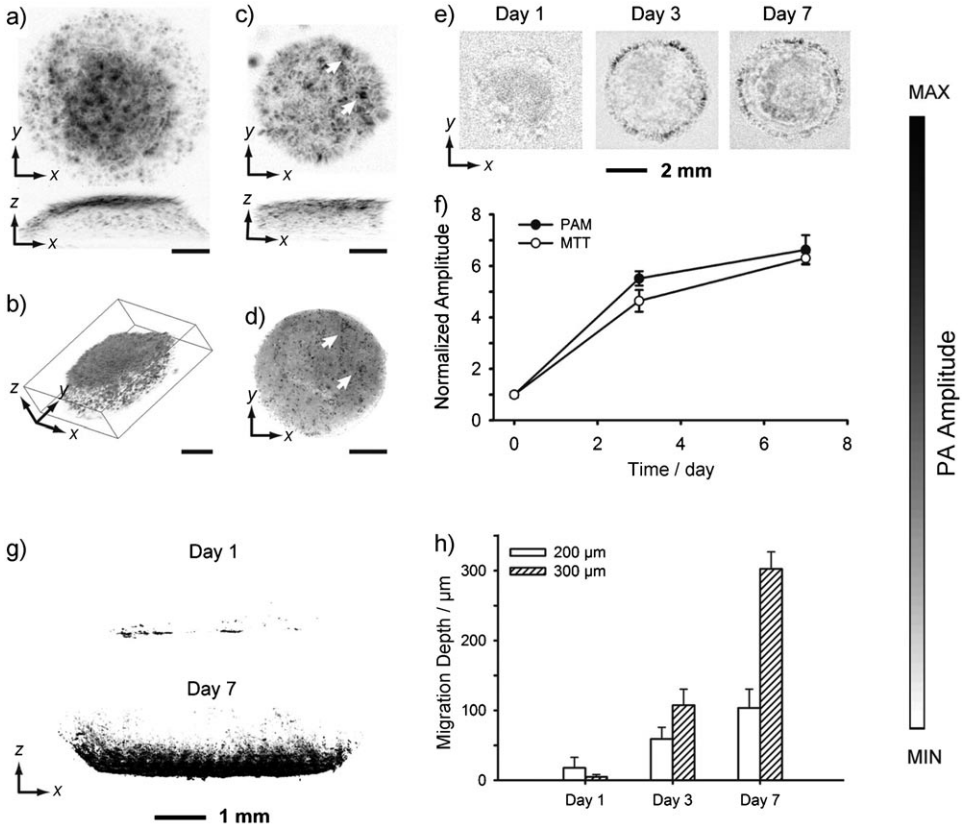

Figure 3. a) PAM maximum amplitude projection (MAP) image of fibroblasts cultured in an inverse opal scaffold, followed by staining with MTT for 3 h; b) 3D rendering of the volumetric PAM data in (a); c) PAM MAP image of fibroblasts cultured in an inverse opal scaffold filled with cross-linked alginate hydrogel, followed by incubation with MTT for 4 h; and d) an optical micrograph showing the same scaffold as in (c). As indicated by arrows, the features in PAM and optical microscopy match well. Scale bars in (a–d): 1 mm. e) PAM chronic images of fibroblasts grown in inverse opal scaffolds (MAPs in the 600–660 μm layers from the top surface) at 6 h, 3 days, and 7 days; f) quantification of cell numbers in the scaffolds as determined by volumetric PAM data and parallel MTT biochemical assays. Data are presented as mean value ± standard deviation ($n=3$). g) PAM images showing cell invasion profile at day 1 and 7 into inverse opal scaffolds with a pore size of 300 μm; h) average cell penetration depths in scaffolds with pore sizes of 200 and 300 μm, respectively, as determined by PAM virtual biopsy. The data are presented as mean value ± standard deviation.

dense matrix rather than the highly porous scaffolds, we filled an inverse opal scaffold with a cell suspension in 1% alginate saline solution, followed by cross-linking with 1% $CaCl_2$ saline solution for 5 min. The cell-laden hydrogel scaffold was kept in culture for 5 days and then subjected to staining with MTT for 4 h. An incubation time of 4 h was chosen so that enough MTT would diffuse into the entire matrix, be up taken and metabolized by the cells to generate MTT formazan. Again, PAM images clearly show identifiable cells throughout the scaffold (Figure 3c). Right after PAM imaging, we took an optical micrograph using a microscope in the reflection mode (Figure 3d). Comparing with the PAM projection images from the top (Figure 3c), well-matched features on the surface of the scaffold were observed as indicated by arrowheads (Figure 3c and d), indicating good accuracy of the PAM technique for cellular imaging.

We then conducted chronic PAM of scaffolds containing the cells, in an attempt to quantify the cell proliferation profile. At 6 h, 3 days, and 7 days post seeding of fibroblasts, the scaffolds were incubated with MTT for 3 h and then imaged with PAM. MAP images from the middle layer (600–660 μm from the top surface) of a typical scaffold at each time point showed the progressive cell proliferation as indicated by the increase in area for the dark dots (Figure 3e). The presence of dark dots with large areas in the center of the scaffold could be attributed to the high cell densities. Quantification could be obtained from the volumetric data of PAM scans. Summations of PA signal amplitudes, which correspond to total cell numbers, measured at day 3 and day 7 were normalized to that obtained at 6 h (Figure 3f). The curve clearly shows how the cells proliferated with time. The proliferation profile that we obtained from PAM correlated well with what was derived from a traditional quantitative MTT cell viability assay. In this case, right after PAM imaging, the formazan crystals were extracted by dissolution with 1-propanol and quantified using a spectrophotometer. The normalized cell proliferation profiles obtained using these two different methods look very similar (Figure 3f).

In addition, a cell invasion experiment was conducted to further expand the scope of application for the staining method in PAM, which essentially functions as virtual biopsy. In this case, we fabricated PLGA inverse opal scaffolds with two different pore sizes of 200 and 300 μm, respectively. After forming monolayers of fibroblasts in a 24-well plate, the scaffolds were carefully placed on top of the cell monolayers (one scaffold per well) and then incubated. The cells were cultured for 1, 3, and 7 days, stained with MTT formazan, and imaged with PAM. As shown by the PAM MAP images taken from the side of the scaffold (Figure 3g), the cells had invaded from the seeding side (bottom of the image) into the scaffold to approximately half of the scaffold thickness in the case of scaffolds with 300 μm pores. The cell invasion depth can be quantified using the volumetric PAM data. The maximum invasion depth was calculated from all the 800 scan slices of PAM for each scaffold (Figure 3h). Scaffolds with small pores (200 μm) showed a faster cell invasion rate than the scaffolds with large pores (300 μm) at day 1. This could be explained by the fact that, for scaffolds with smaller pores, the surface areas and thus the contact regions between the scaffolds and the cell monolayers were larger, facilitating the cell migration in the initial stage. However, as more cells migrated into the scaffolds and started to proliferate, if the windows connecting the pores were not big enough (as in the case of scaffolds with 200 μm pores, where the windows size was 40–50 μm), they might be blocked by the cells, so that further cell invasion was impeded. As expected, scaffolds with 300 μm pores showed deeper invasion at later time points, as they provided bigger windows (70–80 μm) to interconnect adjacent pores for cell migration.

The staining could also enable high-resolution (0.4 μm) PAM imaging. We cultured RW4 mouse embryonic stem cells (mESCs) and SK-BR-3 breast cancer cells on cover glasses and then incubated with MTT for 3 and 1 h, respectively. Both types of cells were shown in details in the images (Figure 4a,b).

As a functional staining dye for live cell, it is important to verify that, after staining with MTT formazan, the cells can still maintain their biological functions and/or form characteristic cell aggregates. Therefore, we investigated the feasibility to stain the same cell lineages by MTT formazan for multiple times during culture. In parallel experimental groups, RW4 and SK-BR-3 cells were incubated with MTT for 3 and 1 h, respectively. After staining, the cells were washed with PBS three times to remove all the remaining MTT, and fresh culture medium was added. At specific time points, the cells were washed again with PBS and subjected to PAM imaging. It was found that almost all the MTT formazan crystals had been released by exocytosis at $t = 3$ h post MTT removal as no PA signals could be detected from the cells. This was also confirmed by observing the cells under an optical microscope. Within the 3 h period, the contrast of the cells became weaker with time, and more needle-like MTT formazan crystals were released by exocytosis and observed to float at the surface of the medium. This procedure was different from what was used in the previous experiment for evolution of MTT metabolism with time in fibroblasts (see Figure S2 in the Supporting Information). In that case, the cells were continuously incubated with MTT, which was not removed until the end of the experiment (12 h in total), so that the formation of MTT formazan was not interrupted. In the new experiment, MTT was removed after incubation with the cells for 3 and 1 h and fresh medium was added. Upon the removal of MTT, the cells stopped producing new MTT formazan, and the formed crystals were cleared out within a certain period of time.

To ensure that formazan crystals were completely released by exocytosis, the cells were further cultured for 36 h post MTT removal while the culture medium was changed every day. After that, RW4 cells were induced to form embryoid bodies (EBs) containing neural progenitors using a 4−/4+ retinoic acid method.[18] For SK-BR-3 cells, multicellular tumor spheroids (MTs) containing around 10^4 cells were formed on methylcellulose hydrogels.[19] The EBs and MTs were imaged with PAM. As expected, both samples did not give detectable PA signals. However, after staining with MTT formazan again, both could be clearly imaged by PAM (Figure 4c,d). More importantly, MAP images from PAM of the middle planes (60 μm in thickness) indicated that

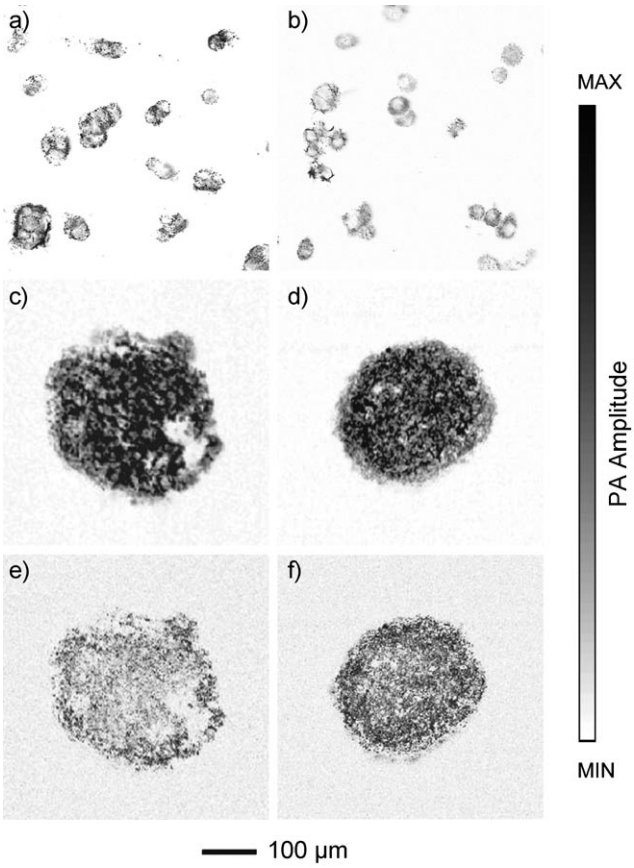

Figure 4. PAM images of a) RW4 mouse embryonic stem cells (RW4 mESCs) and b) SK-BR-3 breast cancer cells incubated with MTT for 3 h. In a parallel experiment, the cells were washed with PBS to remove MTT and fresh medium was added after the same staining procedure with MTT to validate the noninvasive nature of the staining method. The cells were further cultured for 36 h to ensure complete exocytosis of the MTT formazan crystals. The cells were then induced to form characteristic cell aggregates, that is, embryoid bodies in the case of RW4 mESCs or multicellular tumor spheroids in the case of SK-BR-3 breast cancer cells, and then stained with MTT again for PAM. c,d) PAM images of an embryoid body and a multicellular tumor spheroid after staining with MTT. e,f) MAP images taken from the middle planes (60 μm in thickness) of the spheroids shown in (c) and (d), respectively.

MTT can reach the center of the cell body and be metabolized by the cells to form MTT formazan (Figure 4e,f).

Staining with MTT formazan can, in principle, be used to enable high-resolution PAM imaging of all types of metabolically active cells. We have also tested the staining method with several other cell types, including MG63 human osteoblasts, rat bone marrow stromal cells, HepG2 human hepatoma cells, SVEC4-10 mouse endothelial cells, and U-87 MG human brain glioblastoma cells (see Figure S3 in the Supporting Information). We succeeded in visualizing all these cells with the morphology of the whole cell by PAM.

In summary, we have successfully applied staining with MTT to PA imaging of cells containing no natural pigments. Our demonstrations in both 2D and 3D systems indicate that the staining method is well-suited for all types of metabolically active cells, such as fibroblasts, embryonic stem cells, and tumor cells. We have also demonstrated the negligible toxicity of MTT or MTT formazan, making it suitable for noninvasive virtual biopsy with PAM. We anticipate that this method of staining cells for PAM imaging will provide significant insights in visualizing cells for cell biology and tissue engineering. For the present system, MTT formazan crystals have a strong absorption in the region of 500–700 nm. We believe that, by using other tetrazolium–formazan systems, the absorption peak position can be finely tuned[10,12] to enable PAM imaging at other wavelengths for various biological and biomedical applications.

Received: March 8, 2011
Published online: June 16, 2011

Keywords: cancer · imaging agents · photoacoustic microscopy · tissue engineering

[1] M. Xu, L. V. Wang, *Rev. Sci. Instrum.* **2006**, *77*, 041101.
[2] R. M. Weight, J. A. Viator, P. S. Dale, C. W. Caldwell, A. E. Lisle, *Opt. Lett.* **2006**, *31*, 2998.
[3] J.-T. Oh, M.-L. Li, H. F. Zhang, K. Maslov, L. V. Wang, *J. Biomed. Opt.* **2006**, *11*, 034032.
[4] H. F. Zhang, K. Maslov, G. Stoica, L. V. Wang, *Nat. Biotechnol.* **2006**, *24*, 848.
[5] Y. Zhang, C. Xin, S.-W. Choi, C. Kim, L. V. Wang, Y. Xia, *Biomaterials* **2010**, *31*, 8651.
[6] D. Razansky, M. Distel, C. Vinegoni, R. Ma, N. Perrimon, R. W. Köster, V. Ntziachristos, *Nat. Photonics* **2009**, *3*, 412.
[7] L. Li, R. J. Zemp, G. Lungu, G. Stoica, L. V. Wang, *J. Biomed. Opt.* **2007**, *12*, 020504.
[8] W. Lu, Q. Huang, G. Ku, X. Wen, M. Zhou, D. Guzatov, P. Brecht, R. Su, A. Oraevsky, L. V. Wang, C. Li, *Biomaterials* **2010**, *31*, 2617.
[9] D. Pan, M. Pramanik, A. Senpan, S. Ghosh, S. A. Wickline, L. V. Wang, G. M. Lanza, *Biomaterials* **2010**, *31*, 4088.
[10] F. P. Altman, *Prog. Histochem. Cytochem.* **1976**, *9*, 1.
[11] T. Mosmann, *J. Immunol. Methods* **1983**, *65*, 55.
[12] E. Seidler, *Prog. Histochem. Cytochem.* **1991**, *24*, 1.
[13] M. V. Berridge, A. S. Tan, *Arch. Biochem. Biophys.* **1993**, *303*, 474.
[14] *J-Aggregates* (Ed.: K. Takayoshi), World Scientific, Singapore, **1996**.
[15] Y. Wang, K. Maslov, C. Kim, S. Hu, L. V. Wang, *IEEE Trans. Biomed. Eng.* **2010**, *57*, 2576.
[16] S.-W. Choi, J. Xie, Y. Xia, *Adv. Mater.* **2009**, *21*, 2997.
[17] S.-W. Choi, Y. Zhang, S. Thomopoulos, Y. Xia, *Langmuir* **2010**, *26*, 12126.
[18] G. Bain, D. Kitchens, M. Yao, J. E. Huettner, D. I. Gottlieb, *Dev. Biol.* **1995**, *168*, 342.
[19] C.-C. Huang, C.-K. Liao, M.-J. Yang, C.-H. Chen, S.-M. Hwang, Y.-W. Hung, Y. Chang, H.-W. Sung, *Biomaterials* **2010**, *31*, 6218.
[20] C. Zhang, K. Maslov, L. V. Wang, *Opt. Lett.* **2010**, *35*, 3195.

